Annu. Rev. Mater. Sci. 1994. 24:215–34

SURFACE AND INTERFACE STRESSES

Robert C. Cammarata

Department of Materials Science and Engineering, The Johns Hopkins University, Baltimore, Maryland 21218

Karl Sieradzki

Department of Materials and Nuclear Engineering, University of Maryland, College Park, Maryland 20742

KEY WORDS: surface free energy, surface stress, thermodynamics

INTRODUCTION

Perhaps the most fundamental difference (from a thermodynamic point of view) between a solid surface and a liquid surface involves the distinction between the surface free energy and the surface stress. The reversible work per unit area involved in forming a surface, which exposes new atoms, is the surface free energy γ. This parameter describes the reversible work to form a new solid surface by a process such as cleavage. The surface stress f is the reversible work per unit area required to elastically stretch a surface. When a fluid surface is stretched, new atoms or molecules arrive at the surface such that the number of atoms per unit area remains constant. As a result, it can be considered that for a fluid the surface free energy is the same as the surface stress. On the other hand, when a solid surface is elastically stretched, the actual number of atoms per unit area is altered and, in general, $f \neq \gamma$. When a solid of finite size is elastically deformed, work is performed against both volume and surface forces. Under most conditions the volume term will strongly dominate over the surface term. However, for solids of small enough extent, the surface term can become important and induce a bulk stress of order f/t that elastically changes the equilibrium lattice spacing. Here t corresponds to the characteristic length

0084–6600/94/0801–0215$05.00

scale defined by the geometry of the solid that may, for example, correspond to a particle diameter or the thickness of an unsupported thin film. For many materials this effect becomes significant for t smaller than 10 nm.

At the atomic scale, the origin of the surface stress is easily seen in the following argument. Consider a single crystal metal of finite extent. The surface atoms reside in a lower electron density compared to the bulk atoms and therefore wish to adopt an equilibrium spacing different from the bulk. The bulk atoms, however, impose the constraint that the surface atoms are forced into an epitaxial relationship with the underlying lattice. In this sense, the surface atoms are strained, and the surface has a stress exerted on it by the underlying lattice. For low index surfaces of metals, the atoms would prefer to adopt a smaller equilibrium spacing than the bulk in order to increase the local electron density, so that the epitaxial constraint results in a surface tensile stress. (Since the surface is free of normal stresses, relaxations very near the surface will result in a variation of the interplanar spacing perpendicular to the surface.) For a few metals, the constraint imposed by the bulk is energetically too costly, and the surface adopts a lower free energy state by undergoing a reconstruction that increases the surface density of atoms. In many ways this reconstruction is similar to the coherent/incoherent transition of an epitaxial monolayer on a solid substrate first considered by Frank & van der Merwe (1). It will be shown that inclusion of a surface stress term into the standard epitaxy analysis can significantly alter the conventional result for the critical thickness for epitaxy and that a similar approach can be used to model the surface reconstruction.

Any atomistic model that considers only pairwise nearest neighbor central force interactions yields the result that the surface stress equals zero. This was probably first pointed out in a classic paper by Mullins (2), who examined the effect of capillarity on surface morphology. For a pairwise potential that considers just nearest neighbor interactions, the nearest neighbor spacing in the bulk solid occurs at the position corresponding to the energy minimum for the simple pairwise interaction. Such a situation does not produce a sample size-dependent nearest-neighbor spacing and, therefore, results in a zero surface stress. On the other hand, if at least second nearest neighbor interactions are considered, the nearest-neighbor spacing in the bulk occurs at a distance less than the position corresponding to the energy minimum of the pairwise interaction. The lattice parameter then becomes sample size-dependent, which results in a nonzero value of f.

As with the free solid surface, there are stresses associated with solid-solid interfaces (3, 4). Consider a general interface between two solid

phases. There are two different ways in which work can be performed to elastically "stretch" the interface. One way involves equally stretching both phases. This kind of deformation leaves the interface structure unchanged, and the work per unit area involved with the stretching process can be associated with one type of interface stress. Another type of interface stress is associated with the work per unit area required to stretch one phase with respect to the other, which results in an alteration of the interface structure. This way of identifying interface stresses, first given by Cahn & Larché (4), is useful in a discussion of thin film epitaxy.

THERMODYNAMICS OF SURFACE STRESS

In the thermodynamics of surfaces as formulated by Gibbs (5), there is a parameter γ that represents the excess free energy per unit area of a surface. The amount of reversible work dw performed to create new area dA of a fluid or solid surface can be expressed as

$$dw = \gamma\, dA. \qquad 1.$$

In the case of a solid, this new area can be created, for example, by plastic deformation or cleavage. The total work needed to create a planar surface of area A (equivalently, the total excess free energy of the surface) is equal to γA. Gibbs (5) pointed out that in the case of solids, there is a second type of quantity, called the surface stress, that is associated with the reversible work per unit area needed to elastically stretch a pre-existing surface. The relationship between the surface stress and the surface free energy γ can be derived in the following way. The elastic deformation of a solid surface can be expressed in terms of a surface elastic strain tensor ε_{ij}, where $i,j = 1,2$. Consider a reversible process that causes a small variation in the area through an infinitesimal elastic strain $d\varepsilon_{ij}$. The surface stress tensor f_{ij} can be defined such that the work associated with the variation in γA, the total excess free energy of the surface, owing to the strain $d\varepsilon_{ij}$, is equal to (summing over each repeated index):

$$d(\gamma A) = A f_{ij}\, d\varepsilon_{ij}. \qquad 2.$$

Since $d(\gamma A) = \gamma\, dA + A\, d\gamma$, and $dA = A\,\delta_{ij}\, d\varepsilon_{ij}$ (where δ_{ij} is the Kronecker delta), the surface stress f_{ij} can be expressed as

$$f_{ij} = \gamma\delta_{ij} + \partial\gamma/\partial\varepsilon_{ij}. \qquad 3.$$

For a general surface, the surface stress tensor can be referred to a set of principal axes such that the off-diagonal components are equal to zero. For a surface possessing a threefold or higher rotation axis symmetry, the diagonal components are equal, and the surface stress can be taken as a

scalar $f = \gamma + \partial\gamma/\partial\varepsilon$. For most solids, f is generally of the same order of magnitude as γ and can be positive or negative. Both f and γ can be considered as representing a force per unit length, the former exerted by a surface during elastic deformation, and the latter exerted by a surface during plastic deformation. As a result, both f and γ have been referred to as surface tension. This has contributed to some of the confusion concerning the difference between them, and it is probably best to avoid using the term when discussing solid surfaces.

Consider a solid particle with an isotropic surface stress in a surrounding fluid (6). Let the pressure of the solid P_s be different from the pressure of the fluid P_f. At equilibrium, the virtual work $\Delta P\,dV$, where $\Delta P = P_s - P_f$ will equal $f\,dA$, the work performed against the surface stress. For a spherical particle of radius r, this leads to the Laplace-Young Equation for a solid:

$$\Delta P = 2f/r. \qquad 4.$$

It should be noted that the Laplace pressure ΔP for a solid as given in Equation 4 is often incorrectly written as $\Delta P = 2\gamma/r$ (which is the Laplace pressure for a spherical fluid droplet in equilibrium with a different surrounding fluid).

THEORETICAL CALCULATIONS OF SURFACE STRESS

Theoretical calculations of surface stresses generally involve calculating the surface free energy and its derivative with respect to elastic strain. Both first principles calculations and computer simulations involving semi-empirical potentials have been attempted. Theoretical values of the surface stresses for certain solids are given in Tables 1 to 6. It is to be noted that the majority of the surface stresses are positive and of the same order of magnitude as the surface free energy.

Table 1 First principles calculations of surface free energy γ and surface stress f for clean unreconstructed (111) oriented fcc metal surfaces (7–10)

Metal	γ (J/m^2)	f (J/m^2)	Metal	γ (J/m^2)	f (J/m^2)
Al	0.96	1.25	Au	1.25	2.77
Ir	3.26	5.30	Pb	0.50	0.82
Pt	2.19	5.60			

Table 2 Calculated surface free energy γ and surface stress f for clean unreconstructed fcc metal surfaces using embedded atom method potentials (11)

Surface	γ (J/m^2)	f (J/m^2)	Surface	γ (J/m^2)	f (J/m^2)
Ni (100)	1.57	1.27	Au (100)	0.92	1.79
(111)	1.44	0.43	(111)	0.79	1.51
Cu (100)	1.29	1.38	Pt (100)	1.64	2.69
(111)	1.18	0.86	(111)	1.44	2.86
Ag (100)	0.70	0.82			
(111)	0.62	0.64			

Metals

First principles calculations for several clean fcc metal surfaces have been performed by Needs et al (7–10) using a pseudopotential technique that employed a local density approximation for the exchange-correlation energy. Values of the surface free energy and surface stress for unreconstructed (111) oriented fcc metal surfaces are given in Table 1. In order to understand the physical origin of surface stresses in more detail, Needs

Table 3 Calculated surface free energy γ and principal surface stresses f_{xx} and f_{yy} for clean unreconstructed bcc metal surfaces using Finnis-Sinclair potentials (12)

Surface	γ (J/m^2)	f_{xx} (J/m^2)	f_{yy} (J/m^2)
V (100)	1.733	2.424	2.424
(110)	1.473	1.939	0.263
(310)	1.745	2.335	1.255
Nb (100)	1.956	2.532	2.532
(110)	1.669	2.168	0.301
(310)	2.104	2.405	1.267
Ta (100)	2.328	3.249	3.249
(110)	1.980	2.535	0.392
(310)	2.512	3.085	1.647
Mo (100)	2.100	2.241	2.241
(110)	1.829	2.019	0.775
(310)	2.070	2.247	1.184
W (100)	2.924	3.032	3.032
(110)	2.575	2.385	0.271
(310)	3.036	2.833	1.450

For (110) surfaces, x = [1$\bar{1}$0], y = [001]; for (310) surfaces, x = [1$\bar{3}$0], y = [001].

Table 4 Calculated values of the surface stress f for (100) surfaces of alkali halides (13)

Material	f (J/m^2)	Material	f (J/m^2)
LiF	2.287	KCl	0.310
LiCl	1.025	KBr	0.250
LiBr	0.827	KI	0.172
LiI	0.558	RbF	0.427
NaF	1.031	RbCl	0.248
NaCl	0.562	RbBr	0.204
NaBr	0.454	RbI	0.142
NaI	0.303	CsF	0.308
KF	0.549		

Table 5 First principles calculations of surface free energy γ and surface stress f for Si(111) and Ge(111) surfaces (14, 15)

	Surface	γ (eV/1 × 1 cell)	f (eV/1 × 1 cell)
Si	1 × 1	1.45	−0.54
	$\sqrt{3} \times \sqrt{3}$ adatom	1.27	1.70
	2 × 2 adatom	1.24	1.66
Si(Ga)	1 × 1	−3.01	−4.45
	$\sqrt{3} \times \sqrt{3}$	−0.35	1.35
Ge	1 × 1	1.40	−0.73
	2 × 2 adatom	1.20	1.43

Table 6 Calculated values of (111) surface stresses for A and B surfaces of III-V compounds (16)

Material	f_A (J/m^2)	f_B (J/m^2)	Material	f_A (J/m^2)	f_B (J/m^2)
InSb	−0.6	0.3	GaSb	−0.8	0.4
GaAs	−1.0	0.5	AlSb	−0.8	0.4
InAs	−0.7	0.3			

et al (7) calculated the electrostatic, exchange-correlation, and kinetic energy contributions to the surface stress of Al(111). They found that the largest contributor was the term associated with the kinetic energy, while the other two terms were significantly smaller in magnitude and negative.

A similar result was also obtained using a jellium model that had the same average electron density as aluminum. According to Needs et al, this general behavior should be expected for metals with relatively high electron densities, while for metals with lower electron densities such as the alkali metals, it is expected that the electrostatic, exchange-correlation, and kinetic energy terms all contribute significantly to the surface stress.

Calculations of the surface stress for various metals have been made using the embedded atom method (11) and Finnis-Sinclair (12) potentials (see Tables 2 and 3). A comparison of the values of γ and f for Au(111) and Pt(111) given in Tables 1 and 2 shows that the values obtained using the embedded atom method potentials are significantly smaller than those obtained from the first principles calculations.

Ionic Solids

The most commonly studied ionic solid surface stress is that for the (100) oriented surfaces of alkali halides. Table 4 lists values of surface stresses obtained by Nicholson (13).

Semiconductors

First principles calculations using the pseudopotential technique have been performed by Meade & Vanderbilt for (111) oriented surfaces of Si and Ge (14, 15). Values of the surface free energy and the surface stress are listed in Table 5 and are given in the commonly used units of eV per 1×1 cell. In the case of (111) surfaces of compounds such as GaAs and InSb, there is an A type surface, where the terminating plane is composed of Group III atoms, and a B type surface, where the terminating plane is composed of Group V atoms. Cahn & Hanneman (16) performed calculations based on the forces associated with the elastic distortion of the covalent bonds, which they estimated from the bulk elastic constants, in order to estimate the surface stresses of various compounds (see Table 6). It is seen that the A types surface stresses are compressive, while the B type surface stresses are tensile.

EXPERIMENTAL MEASUREMENTS OF SURFACE STRESS

Stresses of all types are generally determined by measuring an elastic strain that results from that stress and then using the appropriate form of Hooke's Law to extract the stress value. This is also true for most surface stress measurements. Consider a small solid sphere of radius r that is presumed to have an isotropic surface stress f. According to Equation 4,

there is a hydrostatic pressure acting on this sphere equal to $\Delta P = 2f/r$ that will induce an elastic strain in the solid. The appropriate form of Hooke's Law is $\Delta P = -3K\varepsilon$, where K is the bulk modulus and ε is the radial strain. The surface stress f can be determined experimentally by measuring the strain as a function of the radius:

$$f = -3K\varepsilon r/2. \quad 5.$$

Vermaak and co-workers (17–19) measured the strain in small spheres of Au, Ag, and Pt by electron diffraction and determined an average surface stress using Equation 5; see Table 7. It is noted that most of these values are within a factor of 2 or so of the theoretical values calculated for a temperature of 0 K given in Tables 1 and/or 2.

A thin rectangular wafer whose top and bottom surface have different surface stresses will bend in response to that difference. By measuring the radius of curvature R of the bent wafer, the difference in the surface stresses of the two surfaces Δf can be calculated using the formula (16)

$$\Delta f = Yt^2/6R, \quad 6.$$

where t is the thickness of the wafer and Y is an elastic modulus that, for an isotropic material, is equal to $E/(1-\nu)$, where E is Young's modulus and ν is Poisson's ratio. Using radius of curvature measurements of (111) oriented InSb wafers obtained by Hanneman et al (20), Cahn & Hanneman (16) obtained a value of Δf of 0.95 to 1.4 J/m^2. This was in good agreement with the difference in the calculated values for the A and B surfaces of InSb given in Table 6.

Martinez et al (21) used the wafer-bending technique to obtain the surface stress of the reconstructed 7×7 Si(111) surface. A submonolayer of Ga was deposited onto one side of a wafer with initially clean Si(111) 7×7 surfaces. The wafer was then heated until the Si(Ga) surface transformed into a $\sqrt{3}\times\sqrt{3}$ structure. As a result, the wafer was observed to bend because of the difference in the surface stresses of the 7×7 and the $\sqrt{3}\times\sqrt{3}$ surfaces, and the measured surface stress difference was 1.02

Table 7 Experimental measurements of surface stress (17–19)

Material	f (J/m^2)	Temperature (°C)
Au	1.175±0.2	50
Ag	1.415±0.3	55
Pt	2.574±0.4	65

eV/(1 × 1 cell). When the theoretical value of 1.35 eV/(1 × 1 cell) for the Si(Ga) $\sqrt{3} \times \sqrt{3}$ surface obtained by Meade & Vanderbilt (see Table 4) is added to this difference, the absolute surface stress of the clean 7 × 7 surface is estimated to be about 2.37 eV/(1 × 1 cell). Schell-Sorokin & Tromp (22) performed similar experiments on Si(100) surfaces and observed wafer curvature due to the difference in the average surface stress between a clean surface and one with adsorbed As or Ge.

INTERFACE STRESSES

As first pointed out by Brooks (3), a general interface has two interface stresses associated with it that correspond to the two solid phases that are separated by the interface. Following Cahn & Larché (4), one can define an interface stress g_{ij} corresponding to the reversible work per unit area needed to strain one of the phases relative to the other, and another interface stress h_{ij} associated with the reversible work per unit area needed to equally stretch both phases.

Interface Stress Associated with Stretching One Phase Relative to the Other

For an interface between two crystals, the strain associated with the interface stress g_{ij} results in a change of the interface structure. For example, consider an epitaxial thin film on a rigid substrate. By changing the misfit dislocation density at the interface, the lattice parameter of the film can be varied while the lattice parameter of the substrate remains fixed. The interface stress g_{ij} can be interpreted as the work per unit area associated with changing the dislocation density. This can be illustrated in the following way (23): Let ε_m be defined as the misfit strain equal to $(a_s - a_f)/a_f$, where a_s and a_f are the bulk lattice parameters of the substrate and film, respectively, and let ε represent the in-plane strain of the film measured with respect to its bulk state. When the film is strained by an amount ε, the strain that is accommodated by misfit dislocations will equal $(\varepsilon_m - \varepsilon)$. Suppose that the misfit dislocations are edge dislocations with their Burgers vectors in the interface and are arranged in a square grid. The interface energy per unit area σ of this dislocation grid can be expressed as (24)

$$\sigma = \sigma_o[1 - (\varepsilon_{11} + \varepsilon_{22})/2\varepsilon_m], \qquad 7.$$

where the strain components $\varepsilon_{11} = \varepsilon_{22} = \varepsilon$, and

$$\sigma_o = Cb|\varepsilon_m|[\ln(t/b) + 1]/2\pi. \qquad 8.$$

In Equation 8, b is the magnitude of the Burgers vector, t is the film thickness, and C is an effective elastic modulus equal to

$2[(1-\nu_f)/G_f+(1-\nu_s)/G_s]^{-1}$, where ν_f and ν_s are Poisson's ratio of the film and substrate, and G_f and G_s are the shear moduli of the film and substrate. Taking the (isotropic) interface stress g as the work per unit area needed to introduce a strain of ε_{11} (holding ε_{22} constant) in a film initially at $\varepsilon_{11}=\varepsilon_{22}=0$ leads to (23)

$$g=\sigma_0+(\partial\sigma/\partial\varepsilon_{11})|_{\varepsilon_{11}=\varepsilon_{22}=0}=\sigma_0[1-1/(2\varepsilon_m)]. \quad 9.$$

For a small misfit strain, it is seen that the interface stress g defined in this manner is opposite in sign to ε_m.

Interface Stress Associated with Stretching Both Phases Equally

In the few studies that have been performed to investigate interface stresses, almost all have been devoted to measuring h_{ij}, the work per unit area needed to stretch an interface by elastically straining both phases on each side of that interface by the same amount e_{ij}. Proceeding in a manner analogous to that used to derive Equation 3, this stress can be related to the interfacial free energy σ by

$$h_{ij}=\sigma\delta_{ij}+\partial\sigma/\partial e_{ij}. \quad 10.$$

Gumbsch & Daw (11) calculated values for this type of interface stress for (100) and (111) noncoherent metal-metal interfaces using standard embedded atom method potentials. Their results are given in Table 8. As was discussed previously, calculations for free solid surfaces using embedded atom method potentials can give values of surface properties significantly smaller than those obtained from first principles calculations. Recently, embedded atom method potentials have been modified so that they give values for the free surface properties approximately equal to those obtained by first principle calculations (25). These potentials are then used to evaluate interface stresses. For the case of a noncoherent

Table 8 Calculations of interface stress h for noncoherent metal-metal interfaces (11)

Bilayer A/B	h for (100) interface (J/m^2)	h for (111) interface (J/m^2)
Ag/Ni	0.83	0.32
Au/Ni	0.71	−0.08
Ag/Cu	0.53	0.32
Au/Cu	0.33	0.01
Pt/Ni	0.04	−0.57

Ag-Ni (111) interface, a value of 1.32 J/m^2 was obtained. This value is significantly larger than that obtained using the standard embedded atom method potentials as given in Table 8.

A few attempts have been made to experimentally measure the interface stress h in layered materials. Crystalline polymers and organic crystals have a lamellar structure and display variations in their lattice parameters that are inversely proportional with lamella thickness. This behavior can be attributed to the effects of an interface stress (26). The physical origin of this interface stress in crystalline polymers can be understood in the following manner. Figure 1 schematically shows a chain-folded molecule in a lamella of a crystalline polymer. In the limit of infinitely long stem lengths, the stems have an equilibrium separation determined by the balance of van der Waals attractive forces and intermolecular repulsive forces. The chain folds are high energy configurations that would attempt to straighten out if they were not constrained by the stems. Thus the chain folds at the interface can be considered under compression, and the interfaces therefore display a negative interface stress.

If the surface stress tensor is referred to the principle axes, the diagonal components h_1 and h_2 can be calculated using the principal strains e_1 and e_2 (26):

$$h_1 = -t(S_{22}e_1 - S_{12}e_2)/(S_{11}S_{22} - S_{12}^2), \qquad 14.$$

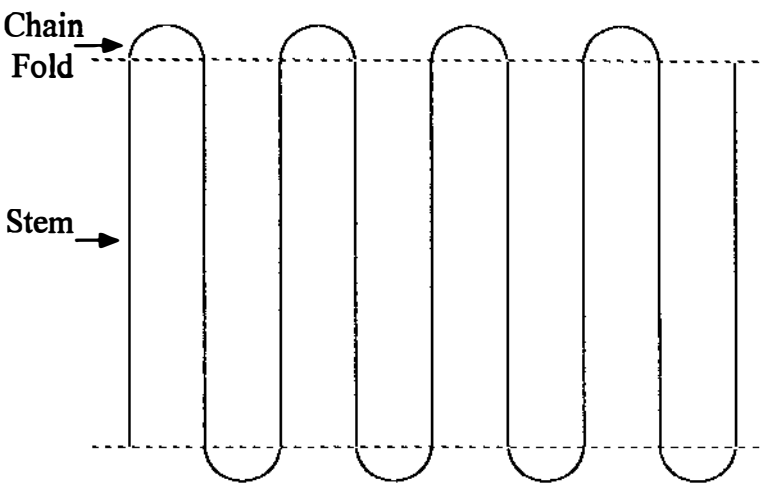

Figure 1 Schematic diagram of a molecule in a crystalline polymer lamella. The chain folds lead to a compressive interface stress.

$$h_2 = -t(-S_{12}e_1 + S_{11}e_2)/(S_{11}S_{22} - S_{12}^2), \quad 15.$$

where t is the lamella thickness, and S_{11}, S_{12} and S_{22} are elastic compliances. Equations 14 and 15 were used to obtain interface stresses for crystalline polymers and n-paraffins (see Table 9).

Ruud et al (27, 28) determined interface stresses in artificially multilayered thin films by measuring the amount of bending the films induce in the substrates. Their results gave $h = 1.13\ \text{J/m}^2$ for the Au(111)/amorphous Al_2O_3 interface and $h = -2.27\ \text{J/m}^2$ for the Ag(111)/Ni(111) interface. It is noted that the experimentally measured value for Ag-Ni is of opposite sign to that predicted theoretically (see Table 8).

Although the discussion has been limited to certain types of boundaries, analogous interface stresses are associated with all types of solid-solid interfaces. If the lattice parameter is a function of the long range order parameter in an ordered alloy, interface stresses associated with the antiphase domain boundaries will result (29). Interface stresses are also expected to be associated with grain boundaries (see Equation 19).

EXAMPLES OF SURFACE AND INTERFACE STRESS EFFECTS

Strains and Elastic Modulus Variations in Nanoscale Materials

Consider the in-plane elastic strains induced by the free surface stress f in a free-standing isotropic thin film of thickness t. The in-plane elastic strain ε generated by the surface stress f of the top and bottom surfaces is

$$\varepsilon = -2f/Yt. \quad 16.$$

Using typical values for metals of $f = 1\ \text{J/m}^2$ and $Y = 10^{11}\ \text{J/m}^3$, a 10 nm film would have an in-plane strain of about -0.2%, while a 2 nm thick film would have a strain of -1%. It is seen that the surface stress can

Table 9 Experimental values of the interface stress h_{ij} in materials that crystallize with a lamellar structure (26)

Material	h_{ij} (J/m^2)	Temperature (°C)
Melt-crystallized polyethylene	−0.414, −0.168	25
n-Paraffins	−0.472, −0.364	23
Random copolymer of tetrafluoroethylene and hexafluoropropylene	−0.2	300

induce an elastic strain greatly in excess of the yield strain obtained by an externally applied stress. These large strains would produce atomic displacements that are well out of the Hookean region of the interactomic potentials, so that higher order elastic effects should be manifested. Theoretical calculations of the in-plane biaxial modulus of Cu(100) as a function of the in-plane strain gives (30):

$$Y(\varepsilon) = Y(0)[1 - B\varepsilon], \qquad 17.$$

where B, which depends on the third order elastic constants, has a value of 15 to 25. Thus a -1% strain should increase the apparent modulus by about 15 to 25%. A more complete analysis gives (25)

$$Y = Y_o + 2f(B + 2\eta - 3 + f'/f)/t, \qquad 18.$$

where Y_o is the modulus value for a bulk material, η is a factor that depends on Poisson's ratio and is close to unity, and f' is equal to $\partial f/\partial\varepsilon$. Calculations of f', which can be considered an "excess surface modulus," have shown that it can be negative (25, 31, 32). For many (100) and (111) oriented fcc metal surfaces, the magnitude of f'/f is significantly smaller than B (25) so that, according to Equation 18, the modulus should always be enhanced when t is reduced below about 5 nm. Although it is not easy to experimentally investigate free standing films with thicknesses less than 5 nm, they can be studied using computer simulations. Elastic strains of order 1% and significant biaxial modulus enhancements were obtained in simulations of ultrathin films (25, 33–35) that were in excellent agreement with Equations 16 and 18.

A similar effect is expected in artificially multilayered (superlattice) thin films owing to interface stress effects (25, 36). In this case, Equations 16 and 18 would still apply, except that f and f' should be replaced with h and h', and t would represent the bilayer repeat length. For systems with sufficiently large interface stresses, strains of order $\pm 1\%$ proportional to $1/t$, and modulus enhancements or reductions (depending on the sign of h) of order 20% are expected when the bilayer thicknesses are reduced below 5 nm. This behavior has been observed experimentally (37). The first experimental reports of modulus variations claimed enhancements of 100% or more (the so-called supermodulus effect). However, the moduli were measured by the bulge test, and it is likely that the apparent modulus enhancements were artifacts of the measurement (38, 39). Recent studies using much more reliable ultrasonic methods indicate that modulus variations involving both enhancements and reductions of order 20% are found for several multilayered metal films such as Cu-Nb (37, 40, 41). Concomitant with these modulus variations are elastic strains proportional to $1/t$ that can be as large as a few percent. Although several theories have

been proposed to explain this behavior, it has been most successfully modeled as a result of interface stress effects (25, 36).

Large elastic strains and modulus variations would also be expected for other types of nanoscale materials (26). If the grains in single phase nanocrystalline materials are modeled as spheres, there will be a strain dependence on the grain size $d = 2r$ analogous to Equation 5 given by

$$\varepsilon = -4h/3Kd, \qquad 19.$$

where h is the interface stress associated with the grain boundaries. Because of higher order elastic effects induced by this strain, the bulk modulus will depend on d (R. Cammarata, in preparation):

$$K(d) = 4h(B_b + h'/h - 1)/3K_o d, \qquad 20.$$

where K_o is the bulk modulus for a bulk material and B_b is the factor for the bulk modulus that is analogous to the factor B for the biaxial modulus in Equation 17.

Surface Stress Effects in Epitaxy of Thin Films

Grabow & Gilmer (42) have considered the thermodynamics of the Frank-van der Merwe (FM) layer-by-layer growth mode, the Volmer-Weber (VW) three-dimensional growth mode, and the Stranski-Krastinov (SK) layer-by-layer followed by three-dimensional growth mode. Their analyses demonstrated that the equilibrium behavior of most real overlayer-substrate systems is dominated by VW or SK behavior, and that the FM growth mode is only favored for systems for which there is zero misfit between overlayer and substrate. For systems characterized by a strong film-substrate interaction, they predict wetting/nonwetting behavior; for a weak film-substrate interaction growth should simply proceed in the form of three-dimensional crystallites. It should be pointed out that careful experimental work on homoepitaxial growth examining Ag on Ag(111) (43) and Pt on Pt(111) (44) has clearly demonstrated that the actual growth mode is often determined by kinetic rather than by thermodynamic considerations.

For well-controlled experimental thin film growth, thermodynamics will provide a lower bound for the critical film thickness that corresponds to the loss of coherency during layer-by-layer growth. A model has been offered (45) that includes a surface stress term in the conventional analysis (24) for the total energy per unit area associated with an overlayer/substrate system. It is found that this extra term significantly alters the predicted critical film thickness. Three separate work terms enter the analysis: the volume elastic energy of a strained overlayer, the work to stretch the film surface, and the work to stretch the interface, which alters

the defect structure of the interface. The elastic energy per unit area can be expressed $Y\varepsilon^2 t$, where Y is the biaxial modulus, t is the film thickness, and ε is the amount of coherency strain in the film. According to Equation 9, the change in the film-substrate interface energy per unit area can be expressed as $2(g-\sigma_o)\varepsilon$. The work per unit area needed to stretch the free surface is $2(\partial\gamma/\partial\varepsilon)\varepsilon = 2(f-\gamma)\varepsilon$. The total work per unit area in a strained overlayer is

$$w = Y\varepsilon^2 t + 2(g-\sigma_o)\varepsilon + 2(f-\gamma)\varepsilon. \quad 21.$$

Note that for $\varepsilon = 0$, $w = 0$, so that the reference state is the completely incoherent overlayer. Most conventional analyses have considered only the first two terms on the right hand side of the equation, ignoring the third term, which gives the contribution of the free surface stress.

The equilibrium strain ε^* is obtained by minimizing w with respect to ε:

$$\varepsilon^* = -(f+g-\gamma-\sigma_o)/Yt. \quad 22.$$

The overlayer thickness at which misfit dislocations first appear is termed the critical thickness t_c and is obtained by setting ε^* equal to the misfit strain ε_m:

$$t_c = -(f+g-\gamma-\sigma_o)/Y\varepsilon_m. \quad 23.$$

Figure 2 is a plot of the critical thickness as a function of the misfit strain (45). Typical values for metals and semiconductors were used to compute the parameters g and σ_o as given by Equations 8 and 9. Curve (*a*) is for the case $\varepsilon_m > 0$ and $f-\gamma = 2.0$ J/m^2, and curve (*c*) is for $\varepsilon_m < 0$ and $f-\gamma = 2.0$ J/m^2. Curve (*b*) is obtained by setting $f = \gamma$ and corresponds to the results of conventional analyses that ignored free surface stress effects. It is seen that when free surface stress effects are included, changing the sign of the misfit strain can greatly change the critical thickness.

Surface Reconstructions of Clean Metal Surfaces

It has recently been observed that clean Pt(111) surfaces reconstruct above 0.65 T_m, where T_m is the melting temperature (46). The reconstruction can be described as a continuous commensurate-incommensurate transformation in which the surface layer is isotropically compressed relative to the underlying lattice. A similar reconstruction above 0.65 T_m has also been reported for Au(111) (47). At lower temperatures, a $23 \times \sqrt{3}$ reconstruction has been observed in Au(111) that can be described as an insertion of an extra row of atoms every 23rd row along the $[1\bar{1}0]$ direction (48). This one-dimensional relaxation represents a surface compression of about

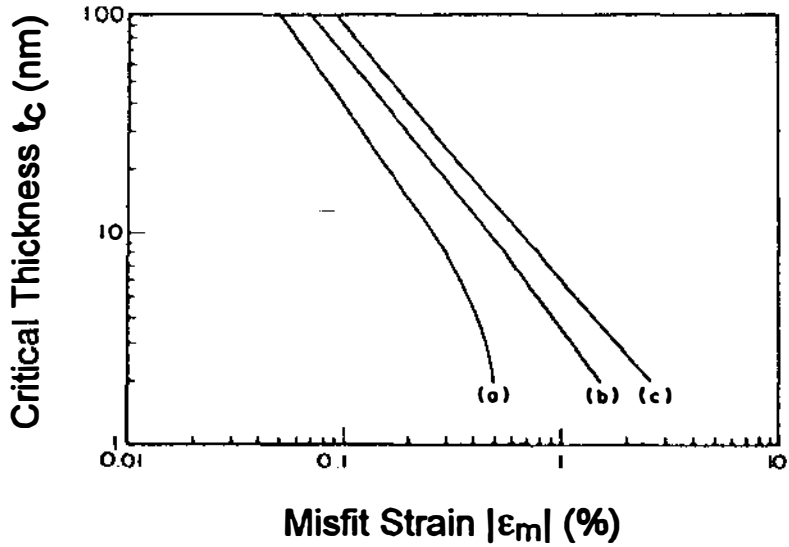

Figure 2 Critical thickness for epitaxy as a function of misfit strain (45). (*a*) $f-\gamma = 2$ J/m^2, $\varepsilon_m > 0$; (*b*) $f-\gamma = 0$; (*c*) $f-\gamma = 2$ J/m^2, $\varepsilon_m < 0$.

4%. All other clean (111) fcc metal surfaces studied (Ir, Al, Ni, etc) have not displayed a surface reconstruction.

Herring (49) proposed a continuum model to analyze surface reconstructions of the type seen in Au(111) and Pt(111) that was recently rederived and extended (50). Consideration will be given first to the one-dimensional compression associated with the low temperature surface reconstruction of Au(111). There are three terms whose sum represents the work per unit area needed to introduce an elastic strain in the top monolayer. First, there is a term that takes into account the elastic energy of the surface layer that is strained by an amount $\varepsilon < 0$ in one direction, but is constrained not to deform in the perpendicular in-plane direction. This elastic energy can be expressed as $E\varepsilon^2 t/2(1-\nu^2)$, where t is the surface layer thickness. The second term is associated with the energy of the noncoherent interface between the strained surface atoms and the underlying lattice. This term can be taken as the energy needed to form a periodic row of surface edge dislocations that accommodates the in-plane misfit strain ε and can be expressed (50) as $\alpha Gb|\varepsilon| = -\alpha Gb\varepsilon$, where G is the shear modulus and $\alpha \approx [4\pi(1-\nu)]^{-1}$, where ν is Poisson's ratio. The third term gives the change in the surface free energy owing to the elastic strain

ε and resulting change in the surface density of atoms. This energy change can be expressed as $\partial\gamma/\partial\varepsilon\,\varepsilon = (f-\gamma)\varepsilon$. The total work per unit area associated with the one-dimensional transformation from an ideal 1×1 surface to a reconstructed surface of strain ε can be written as

$$w = Et\varepsilon^2/2(1-\nu^2) - \alpha Gb\varepsilon + (f-\gamma)\varepsilon. \quad 24.$$

The total work associated with a two-dimensional compression can be expressed as

$$w = Yt\varepsilon^2 - 2\alpha Gb\varepsilon + 2(f-\gamma)\varepsilon, \quad 25.$$

where Y is the biaxial modulus, and the factors of 2 reflect the two-dimensional nature of the strain. It is to be noted that Equation 25 is essentially the same as Equation 21 when the misfit strain ε_m is set equal to zero.

For both the one-dimensional and two-dimensional transformations, an instability criterion can be established by setting $w < 0$. Restricting attention to the onset of the reconstruction process ($\varepsilon \to 0$) leads to the following condition for the surface to be unstable (49, 50):

$$(f-\gamma)/Gb > \alpha. \quad 26.$$

When $\beta \equiv (f-\gamma)/Gb$ is less than the critical value $\alpha \approx 0.1$, the unreconstructed surface is stable; if β exceeds the critical value, the surface is predicted to reconstruct.

The instability criterion developed above will now be compared to experimental observation. Consideration is given to the set of metals found in Table 1. The parameter β was computed (50) for each surface using the values of the surface free energy and the surface stress given in Table 1 and is given in Table 10. As can be seen, the criterion $\beta > 0.1$ correctly predicts that Au and Pt should display reconstructions, while Al and Ir should have stable 1×1 surfaces. Although Au and Ir have about the same driving force for surface reconstruction, equal to $(f-\gamma)$, Ir has a shear modulus almost an order of magnitude larger than that of Au. As a result, the opposing force for reconstruction, the energy to create a noncoherent

Table 10 Calculated values for the stability parameter β for clean (111) fcc metal surfaces (50)

Metal	β	Metal	β
Al	0.041	Au	0.19
Ir	0.034	Pb	0.17
Pt	0.19		

interface, is large enough to keep the unreconstructed surface of Ir stable, but small enough to allow Au to reconstruct. From the model it is possible to derive an expression for the equilibrium amount of elastic strain associated with the reconstruction by setting $\partial w/\partial \varepsilon = 0$. From Equation 24 the equilibrium strain for the one-dimensional compression is

$$\varepsilon = (\alpha Gb + \gamma - f)(1 - \nu^2)/Et. \qquad 27.$$

Using Equation 27, a calculation for the strain in the low temperature reconstruction of Au gives $\varepsilon = -3\%$. This can be considered in reasonable agreement with the experimental value of -4%. The model also predicts that the Pb(111) surface should reconstruct. The clean (111) surface of Pb has not been studied in detail, so it is not known if it displays the predicted reconstruction.

Other metal surface reconstructions can be attributed to surface stress effects. The stability criterion $(f-\gamma)/Gb > \alpha$ successfully predicts reconstructions in clean fcc metal (100) surfaces (50). Au(110) reconstructs into a "missing row" structure that can be described as resulting from removing every other row of atoms from the top monolayer. An explanation for this behavior has been offered by Dregia et al (32). When the sum of the surface stress f and the "surface modulus" f' is less than zero, there is a driving force for the surface to buckle. Computer simulations using embedded atom potentials indicate that $f+f'$ is less than zero for the ideal Au(110) surface, and the predicted periodicity of the buckling is close to the value of two interatomic distances characteristic of the missing row reconstruction.

It has recently been suggested (51) that every surface for which $f \neq \gamma$ should display a reconstruction of the type discussed for (111) oriented surfaces of Au and Pt. However, it is correct to say only that when $f \neq \gamma$, there is a driving force for reconstruction. In most cases the opposing force, equal to the energy cost associated with the surface monolayer losing structural coherence with the underlying lattice, is too large to make the reconstruction thermodynamically favorable (7, 50, 52, 53). Except for the examples cited above, it is not clear what role if any the surface stress plays in other types of reconstructions. In the case of (111) oriented Si, Vanderbilt (54) has shown that the 7×7 structure is more stable than the ideal 1×1 structure because of dangling bond reductions despite surface stress effects that actually oppose the reconstruction.

ACKNOWLEDGMENTS

The authors would like to thank SM Prokes, FH Streitz, JW Cahn, F Spaepen, and TM Trimble for stimulating discussions. RCC also gratefully acknowledges support from the National Science Foundation under grant

number ECS-920222 and the Office of Naval Research under grant number N00014-91-J-1169.

Literature Cited

1. Frank FC, van der Merwe JH. 1949. *Proc. R. Soc. London Ser. A* 198: 205
2. Mullins WW. 1963. In *Metal Surfaces: Structure, Kinetics and Energetics*, p. 17. Metals Park, Ohio: Am. Soc. Metals
3. Brooks H. 1963. In *Metal Interfaces*, p. 20. Metals Park, Ohio: Am. Soc. Metals
4. Cahn JW, Larché F. 1982. *Acta Metall.* 30: 51
5. Gibbs JW. 1906. *The Scientific Papers of J. Willard Gibbs*, Vol. 1, p. 55. London: Longmans-Green
6. Cahn JW. 1980. *Acta Metall.* 28: 1333
7. Needs RJ, Godfrey MJ, Mansfield M. 1991. *Surf. Sci.* 242: 215
8. Needs RJ, Mansfield M, 1989. *J. Phys. Cond. Matter* 1: 7555
9. Needs RJ, Godfrey MJ. 1990. *Phys. Rev. B* 42: 10933
10. Mansfield M, Needs RJ. 1991. *Phys. Rev. B* 43: 8829
11. Gumbsch P, Daw M. 1991. *Phys. Rev. B* 44: 3934
12. Ackland GJ, Finnis MW. 1986. *Philos. Mag. A* 54: 301
13. Nicholson MM. 1955. *Proc. R. Soc. London Ser. A* 228: 490
14. Meade RD, Vanderbilt D. 1989. *Phys. Rev. B* 40: 3905
15. Meade RD, Vanderbilt D. 1989. *Phys. Rev. Lett.* 63: 1404
16. Cahn JW, Hanneman RE. 1964. *Surf. Sci.* 1: 387
17. Mays CW, Vermaak JS, Kuhlmann-Wilsdorf D. 1968. *Surf. Sci.* 12: 134
18. Wassermann HJ, Vermaak JS. 1970. *Surf. Sci.* 22: 164
19. Wassermann HJ, Vermaak JS. 1972. *Surf. Sci.* 32: 168
20. Hanneman RE, Finn MFC, Gatos HC. 1962. *J. Phys. Chem. Solids* 23: 1553
21. Martinez RE, Augustyniak WM, Golovchenko JA. 1990. *Phys. Rev. Lett.* 64: 1035
22. Schell-Sorokin AJ, Tromp RM. 1990. *Phys. Rev. Lett.* 64: 1039
23. Cammarata RC. 1993. *Prog. Surf. Sci.* In press
24. Matthews JW, ed. 1975. *Epitaxial Growth*, p. 559. New York: Academic
25. Streitz FH, Cammarata RC, Sieradzki K. 1993. *Phys. Rev. B* In press
26. Cammarata RC, Eby RK. 1991. *J. Mater. Res.* 6: 888
27. Ruud JA, Witrvrouw A, Spaepen F. 1991. *Mater. Res. Soc. Symp. Proc.* 209: 737
28. Ruud JA, Witrvrouw A, Spaepen F. 1993. *J. Appl. Phys.* 74: 2517
29. Cahn JW. 1986. *Acta Metall.* 37: 713
30. Banerjea A, Smith JR. 1987. *Phys. Rev. B* 35: 5413
31. Price CW, Hirth JP. 1976. *Surf. Sci.* 57: 509
32. Dregia SA, Bauer CL, Wynblatt P. 1987. *J. Vac. Sci. Technol. A* 5: 766
33. Wolf D, Lutsko JF. 1988. *Phys. Rev. Lett.* 60: 1170
34. Dodson BW. 1988. *Phys. Rev. Lett.* 60: 2288
35. Streitz FH, Cammarata RC, Sieradzki K. 1990. *Phys. Rev. B* 41: 12285
36. Cammarata RC, Sieradzki K. 1989. *Phys. Rev. Lett.* 62: 2005
37. Cammarata RC. 1993. In *Mechanical Properties and Deformation Behavior of Materials Having Ultrafine Microstructures*, ed. M Nastasi, DM Parkin, H Gleiter, p. 193. Dordrecht: Kluwer Academic
38. Itozaki H. 1982. PhD thesis. *Mechanical properties of composition modulated copper palladium foil.* Northwestern Univ.
39. Baker SP, Small MK, Vlassak JJ, Daniels BJ, Nix WD. 1993. See Ref. 37, p.165
40. Fartash A, Fullerton EE, Schuller IK, Bobbin SE, Wagner, JW, et al. 1991. *Phys. Rev. B* 44: 13760
41. Schuller IK, Fartash A, Grimsditch M. 1990. *MRS Bull.* XV: 33
42. Grabow MH, Gilmer GH. 1988. *Surf. Sci.* 194: 333
43. van der Vegt HA, van Pinxteren HM, Lohmeier M, Vlieg E, Thornton JMC. 1992. *Phys. Rev. Lett.* 68: 3335
44. Kunkel R, Poelsema B, Verheij LK, Comsa G. 1990. *Phys. Rev. Lett.* 65: 733

45. Cammarata RC, Sieradzki K. 1989. *Appl. Phys. Lett.* 55: 1197
46. Sandy AR, Mochrie SGJ, Zehner DM, Grubel G, Huang KG, Gibbs D. 1992. *Phys. Rev. Lett.* 68: 2192
47. Huang KG, Gibbs D, Zehner DM, Mochrie SGJ. 1990. *Phys. Rev. Lett.* 65: 3313
48. Harten U, Lahee AM, Toennies JP, Woll Ch. 1985. *Phys. Rev. Lett.* 54: 2619
49. Herring C. 1951. In *The Physics of Powder Metallurgy*, ed. WE Kingston, p. 143. New York: McGraw-Hill
50. Cammarata RC. 1992. *Surf. Sci.* 279: 341
51. Wolf D. 1993. *Phys. Rev. Lett.* 70: 627
52. Needs RJ. 1993. *Phys. Rev. Lett.* 71: 460
53. Chou MY, Wei S, Vanderbilt D. 1993. *Phys. Rev. Lett.* 71: 461
54. Vanderbilt D. 1987. *Phys. Rev. Lett.* 59: 1456

Annual Review of Materials Science
Volume 24, 1994

CONTENTS

(*continued*)